Providing the broadest portfolio of flow cytometry controls

Offering the broadest portfolio of peripheral blood controls for immunophenotyping by flow cytometry

- Offering a wide portfolio of intracellular and surface marker controls for flow cytometry
- Unique controls for normal and abnormal leukocyte populations
- Ready to use controls with no dilution required
- Reference values similar to those found in relevant blood types
- Covering CD markers for TBNK, Stem Cells, and Leukemia and Lymphoma

Looking out for the lab.

streck.com

STRECK

Cytometry PART A
ISAC Journal of Quantitative Cell Science

Quantitative Chromogenic Immunohistochemical Image Analysis in CellProfiler Software

V. Tollemar,[1†] N. Tudzarovski,[1†] E. Boberg,[2] A. Törnqvist Andrén,[2] A. Al-Adili,[3] K. Le Blanc,[2] K. Garming Legert,[1] M. Bottai,[4] G. Warfvinge,[5] R.V. Sugars[1*]

[1]Division of Oral Diagnostics and Rehabilitation, Department of Dental Medicine, Karolinska Institutet, Huddinge, Sweden

[2]Division of Clinical Immunology and Transfusion Medicine, Department of Laboratory Medicine, Karolinska Institutet, Stockholm, Sweden

[3]Department of Oral and Maxillofacial Surgery, Karolinska University Hospital, Stockholm, Sweden

[4]Unit of Biostatistics, Institute of Environmental Medicine, Karolinska Institutet, Stockholm, Sweden

[5]Department of Oral Pathology, Faculty of Odontology, Malmö University, Malmö, Sweden

Received 18 March 2018; Revised 14 July 2018; Accepted 16 July 2018

Grant sponsor: Karolinska Institutet; Grant sponsor: The Styrgruppen KI/SLL för Odontologisk Forskning (SOF); Grant sponsor: Stockholm County Council; Grant sponsor: The Swedish Dental Society;

Additional Supporting Information may be found in the online version of this article.

[†]These authors have contributed equally to this manuscript

[*]Correspondence to: Rachael V. Sugars, Division of Oral Diagnostics and Rehabilitation, Department of Dental Medicine, Karolinska Institutet, Alfred Nobel's Allé 8, 14104 Huddinge, Sweden, Email: rachael.sugars@ki.se

Published online 00 Month 2018 in Wiley Online Library (wileyonlinelibrary.com)

DOI: 10.1002/cyto.a.23575

Abstract

Visual grading of chromogenically stained immunohistochemical (IHC) samples is subjective, time consuming, and predisposed to considerable inter- and intra-observer variations. The open-source digital analysis software, CellProfiler has been extensively used for fluorescently stained cells/tissues; however, chromogenic IHC staining is routinely used in both pathological and research diagnostics. The current investigation aimed to compare CellProfiler quantitative chromogenic IHC analyses against the gold standard manual counting. Oral mucosal biopsies from patients with chronic graft-versus-host disease were stained for CD4. Digitized images were manually counted and subjected to image analysis in CellProfiler. Inter-observer and inter-platform agreements were assessed by scatterplots with linear regression and Bland–Altman plots. Validation comparisons between the manual counters demonstrated strong intra-observer concordance (r^2 = 0.979), particularly when cell numbers were less than 100. Scatterplots and Bland–Altman plots demonstrated strong agreement between the manual counters and CellProfiler, with the number of positively stained cells robustly correlating (r^2 = 0.938). Furthermore, CellProfiler allowed the determination of multiple variables simultaneously, such as area stained and masking to remove any non-stained tissue and white gaps, which also demonstrated reliable agreement (r^2 = >0.9). CellProfiler demonstrated versatility with the ability to assess large numbers of images and allowed additional parameters to be quantified. CellProfiler allowed rapid high processing capacity of chromogenically stained chronic inflammatory tissue that was reliable, accurate, and reproducible and highlights potential applications in research diagnostics. © 2018 International Society for Advancement of Cytometry

Key terms

chromogenic; immunohistochemistry; oral mucosa; image analysis; CellProfiler

Introduction

With the movement toward personalized diagnostics and novel treatment options in the fields of cancer and inflammatory diseases, the use of digital pathology scanning systems with adjunctive image analysis tools has rapidly gained momentum in recent years (1–3). Immunohistochemistry (IHC), as an aid to histopathological analyses, provides auxiliary information concerning spatial distribution and magnitude of cells or biomarkers within a tissue. In addition to stated descriptive terms, such as "band-like," "heavy," and "absent," current pathological routines typically involve subjective visual manual assessment of IHC-stained specimens that are graded by percentage or via contrived groups such as –, +, ++, and +++ (4). However, these nonstandardized evaluations remain a challenge even to an experienced pathologist and ultimately diagnostics may suffer from subjectivity, which may influence clinical outcome (4). Many research reports still apply manual scoring as the golden standard to withdraw quantitative data from IHC, which makes inter-study comparisons difficult and requires validation by more than one observer to reduce variation in a

ISAC International Society for Advancement of Cytometry

time consuming practice (1,4,5). Therefore, computer-aided diagnostics offer significant advantages to pathologist working practices to provide reproducible, reliable, and accurate diagnostic assessments of tissue specimens and to move IHC from a qualitative/semiquantitative technique to more robust quantitative outputs (6).

When establishing IHC image analysis routines, a number of factors need to be taken into consideration in order to develop robust reproducible procedures, in particular ensuring standardized sample preparation, the IHC protocol stages, and associated signal development (5). All of these factors can have a significant influence on the outcome. Most routine clinical pathology laboratories employ chromogenic detection methods, in particular 3,3′-diaminobenzidine (DAB) together with nuclear staining by haematoxylin. Therefore, within an image analysis system, identification of the chromogenic dye together with the nuclear stain is paramount. Image analysis should support and not complicate the work of the pathologist. A large number of image analysis systems are currently available associated with robust staining platforms (reviewed by (2)). In the current investigation, we have employed the use of the freely downloadable open-source software CellProfiler (7).

CellProfiler is a multipurpose software that has numerous advantages to already existing image analysis programs (7,8). Designed for biologists, CellProfiler performs multiple sample analyses simultaneously, providing a high-throughput platform without the need to adjust the configuration or the user to possess programming skills. CellProfiler has been widely used for a variety of biological applications from the measurement of cell size and assessment of cell morphology to assays determining wound healing (9–12). Most frequently, this system has been published supporting the quantification of fluorescently stained microscopy specimens. To our knowledge, CellProfiler has only been used for chromogenic quantification in two recent reports (13,14). Herein, we demonstrate and validate the value of this system for the identification and quantification of DAB chromogenically stained IHC tissues.

Using CD4 IHC-stained oral buccal mucosal biopsies from patients with chronic graft-versus-host disease (cGvHD), we primarily assessed the potential of CellProfiler to count chromogenically stained cells against routinely used manual counting for total cell number. As a secondary outcome, we have also determined the total area stained as a reflection of marker distribution within CellProfiler. Due to the possibility of downloading published CellProfiler pipelines for others to use, we show the methodology and validation for future researchers to use. We propose that CellProfiler may significantly contribute to the use of computer-aided image analyses for quantification of chromogenic IHC staining in research and pathology.

Materials and Methods

Patient Material

The 5-mm buccal mucosa punch-biopsies adjacent to lesion sites close to the second molar were retrieved from 10 patients with oral cGVHD attending the Oral Medicine Clinic at Karolinska University Hospital for routine posthematopoietic stem cell transplantation check-ups and five healthy patients undergoing oral surgery (Supporting Information) (15,16). All studies were performed in accordance with the Declaration of Helsinki and permission from Stockholm Local Ethics Board (Dnr: 2012/2235–31/4). Tissues were fixed in formalin (~8 h) before processing for paraffin embedding, and 3 μm thin sections were mounted on SuperFrost Plus slides (Menzel-Gläser, Braunschweig, Germany).

CD4 IHC

Rehydrated sections were treated with heat antigen retrieval using basic buffer pH 9 (R&D Systems, London, UK) at 100°C for 10 min and cooling to room temperature (RT). Following treatment with 3% H_2O_2 for 5 min at RT, nonspecific binding was blocked for 1 h at RT using 10% normal goat serum (NGS; DAKO Glostrup, Denmark), 0.3% Triton-X®-100 (Sigma-Aldrich, Stockholm, Sweden), and 0.1% cold-water fish gelatin (Sigma-Aldrich). Slides were incubated overnight with monoclonal rabbit anti-CD4 human antibody (1:8,000; Abcam, Cambridge, UK) or rabbit IgG isotype control (Vector Laboratories, Burlingame, CA). Biotinylated goat anti-rabbit IgG (1:500, DAKO) was incubated for 1 h at RT followed by antibody enhancement using ABC Elite Kit Reagent (Vector) for 30 min. Bound antibodies were detected using DAB (DAKO), and the tissue was counterstained with Mayer's Hematoxylin (HTX; Histolab Products AB, Gothenburg, Sweden) before dehydration and mounting in Pertex® (Histolab).

Digital Imaging Acquisition and Image Segmentation

Immunohistochemically stained samples were digitalized using the 3D Histech Midi Scanner System and viewed within the Panoramic Viewer Software 1.15 (Histolab Products AB). These scanned slides were used for the acquisition of the manual images evaluated by visual counting and image analysis. The original scanned images were annotated with a straight line to exclude the submucosa and to define the lower region of the reticular layer of the lamina propria, using Case Viewer (Histolab Products AB) (Figure 1). The mucous membrane was included for further image segmentation. Regions (RAW) above the straight line were included in the representation of the fields of view (FoV) for analysis. Image acquisition was established by one team member not involved in the counting process using box annotations to form an image grid in CaseViewer (Figure 1). Multiple FoV were taken from the annotated RAW regions by one team member using the CaseViewer software and coded. A minimum of six (average 20) FoV were taken from each region, covering the defined mucous membrane at ×30 magnification on a 1594 × 768 sized screen = 797 × 392 dots per inch (dpi)/image (Supporting Information).

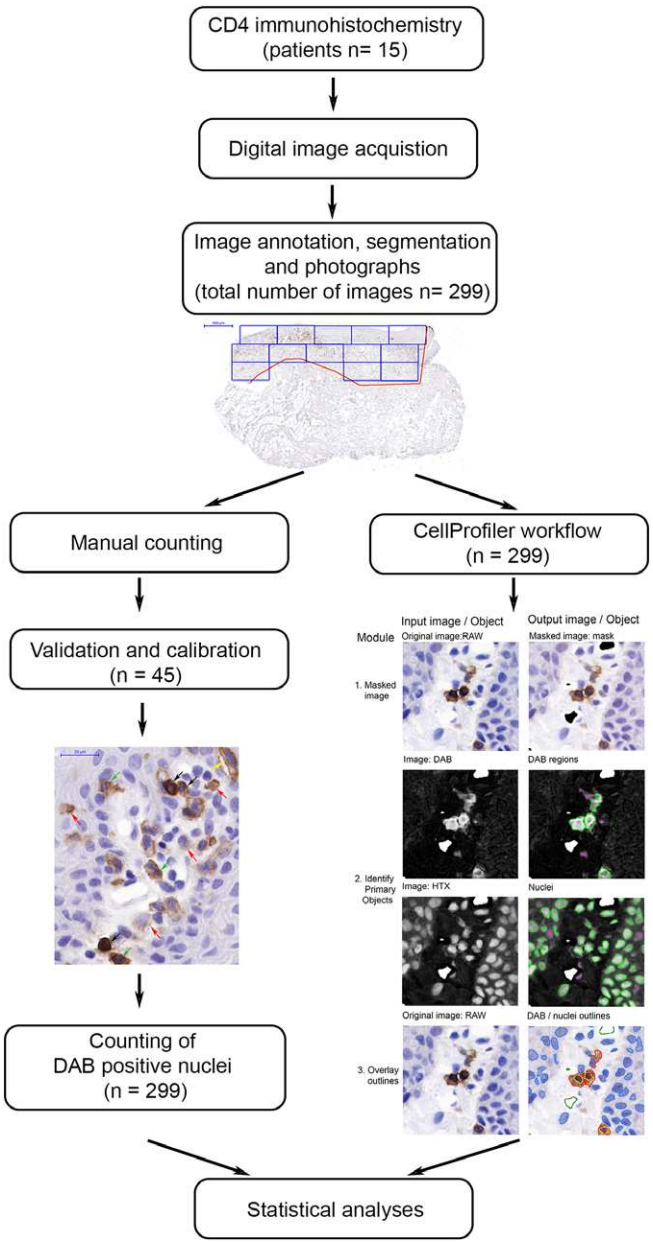

Figure 1. Overview of the analytical process. Flow diagram summarizing the workflow of the study. Oral cGVHD and healthy control sections (n = 15) were immunohistochemically stained against CD4 and digitalized prior to analysis. Manual counting and digital image analysis of segmented images from individual biopsies. Scanned images were annotated to exclude submucosa and to define the lamina propria reticular layer (red line). Regions on or above the annotation were included and images acquired using box annotations (blue squares). The images were segmented (n = 299) and subjected to both manual and quantitative image analysis. Manual counting validation (n = 45) was performed by four researchers for DAB-positive nuclei. These were considered positive when DAB stained around HTX-stained nuclei (black arrow). Cells that lacked nuclei but were DAB positive (green arrow) were excluded, as were cells touching the right and top edges (yellow arrow) and those that were too weak or nonspecific (red arrow). Single cells were distinguished from clusters based on shape and staining appearance. Following validation remaining DAB-positive nuclei were counted (n = 254). A quantitative image analysis pipeline was established in CellProfiler and applied to all 299 images simultaneously. The pipeline consisted of 12 modules (fully detailed in the Supporting Information). The RAW original images were masked (1) to exclude any white regions. The colored images were converted to gray scale and DAB regions and nuclei were identified (2). The identified DAB-stained regions (red outline), nuclei (blue outline), and DAB-positive nuclei (yellow outlines) were overlaid onto the original RAW image. Scale bars: 500 and 20 μm. [Color figure can be viewed at wileyonlinelibrary.com]

Visual Manual Cell Counting

All coded images obtained from manual segmentation were assessed using visual counting (n = 299). Validation and inter-evaluator calibration was performed by four researchers (counters 1–4) with varying degrees of experience but included an oral pathologist. A validation protocol using

selected images was established by a fifth independent researcher stipulating standardized conditions and thresholds for inclusion by which visual counting should be performed; consistently on the same large screen (~42 in. screen) within a darkened room and that the pixel size should mirror the computer on the large screen. Images were viewed within Adobe Photoshop® (Adobe Systems Incorporated, San Jose, CA), and DAB-positive counted cells were recorded using the counting tool. Cells were considered as positive for DAB staining surrounded a HTX-stained nuclei (Figure 1). Cells touching the right and top edges were excluded, and single cells were distinguished from clusters based on shape and staining appearance in accordance above. Forty-five images were randomly selected by the team member not involved in the counting process. The counts were recorded on a spreadsheet, and all counted images were saved for inter-expert evaluation. Final manual counting of all remaining images was divided equally between three researchers (counters 1–3) (n = 254) based on the validation protocol.

Quantitative Image Analysis

Image analysis was performed on the manually acquired FoV-segmented images (RAW) using the open-access CellProfiler Software version 2.2.0 (www.cellprofiler.org) (7). Workflows were established for the CD4 antibody adding preprogrammed algorithmic modules in a pipeline (Figure 1 and Supporting Information). The pipeline can be freely downloaded from http://cellprofiler.org/examples/published_pipelines. Ten images were randomly selected from the manual counters' validation set to act as representative images in the development of the pipeline and to obtain identification thresholds for the stained objects. First, any white regions, such as edges of biopsies, tears, or gaps within the tissue were excluded and applied to mask the RAW image (Figure 1, 1). The masked RAW image was converted to gray scale for the identification of stained objects (DAB and nuclei). Filters were separately applied to identify DAB- and HTX (nuclei)-stained objects using threshold algorithms (Figure 1, 2) (17). Identified DAB and nuclei objects were overlaid onto the RAW images and manually inspected to facilitate program optimization settings (Figure 1, 3). Numerous measurements were made in parallel on the identified objects, including total number of DAB and nuclei stained cells, the total number of DAB-positive nuclei (Positive Cells-CellProfiler), the number of DAB stained regions (DAB regions), total DAB stained pixel area (DAB area), and total stained pixel area per total pixel area (DAB area masked) analyzed. All manually acquired images (n = 299) were processed.

Statistical Methods

Concordance was assessed across the four counters by calculating the intra-image correlation and its 95% confidence interval (18–20). Positive cell counts in each image were measured by the counters and identified objects by CellProfiler. Inter-observer correlations were determined from scatterplots with a linear association between all pair combinations of manual and CellProfiler by fitting simple linear regression models. Standard errors were estimated with the sandwich estimator, which was robust to misspecifications of the linear regression model assumptions (21). The data were presented as fitted regression lines with 95% confidence forecast bands and coefficient of determination (R-squared). Inter-platform agreement between the different methods of manual counting and image analysis was further assessed using Bland–Altman plots (11,22,23). The data were calculated using the difference between the results from Positive Cells-Manual (combined [counters 1–3] or individually [counters 1–4]) and Positive Cells-CellProfiler or DAB-regions-CellProfiler against the mean of the two measurements (22). The data were presented with $\pm$1.96 standard deviations (s). Strong agreement was determined if ~95% of data points laid within $\pm$1.96 s of the mean. All analyses and plots were performed in Stata version 15 (StatCorp, TX).

Results

Concordance Between Manual Counters for DAB-Positive Cells in the Validation Set

A total of 45 randomly selected CD4-stained images were counted by four counters according to the validation protocol. Each had varying levels of experience from a senior researcher (counter 1) and the "gold-standard" oral pathologist (counter 4) to less experienced researchers (counters 2 and 3 respectively). No significant variation was found between the four counters using intra-class correlation (r^2 = 0.979) and between the three counters that continued to count all images (r^2 = 0.981). The greatest discrepancies were observed in those images with greater than 100 cells (Figure 2). Overall, there was a strong pairwise correlation across all counters, which was further supported in the estimated 95% confidence intervals for the pairwise comparisons that overlapped for all four (Figure 2, Table 1, and Supporting Information). The remaining images (n = 254) were randomly distributed into three groups and counted individually by counters 1–3, and 45 images from the validation set were randomly selected for inclusion into the final statistical analyses.

Concordance Between Manual Counting and Digital Image Analysis of Positive Cells-CellProfiler

The whole image set (n = 299) was subjected to concurrent analysis within the optimized CellProfiler pipeline to determine the total number of DAB-positive nuclei (Positive Cells-CellProfiler). Scatterplots and Bland–Altman plots were used to assess inter-observer and inter-platform agreement respectively. A strong correlation was seen for the inter-observer analyses between the Positive Cells-Manual and the Positive Cells-CellProfiler and DAB-regions-CellProfiler (r^2 = 0.938 and 0.927, respectively) (Figure 3A, Table 2, and Supporting Information). Bland–Altman plots demonstrated that for both Positive Cells-CellProfiler and DAB-regions-CellProfiler, the majority of points laid within the specified limits (94%) and that there was a similar difference between 1.96 s compared to the manual counters (Figure 3A and Supporting

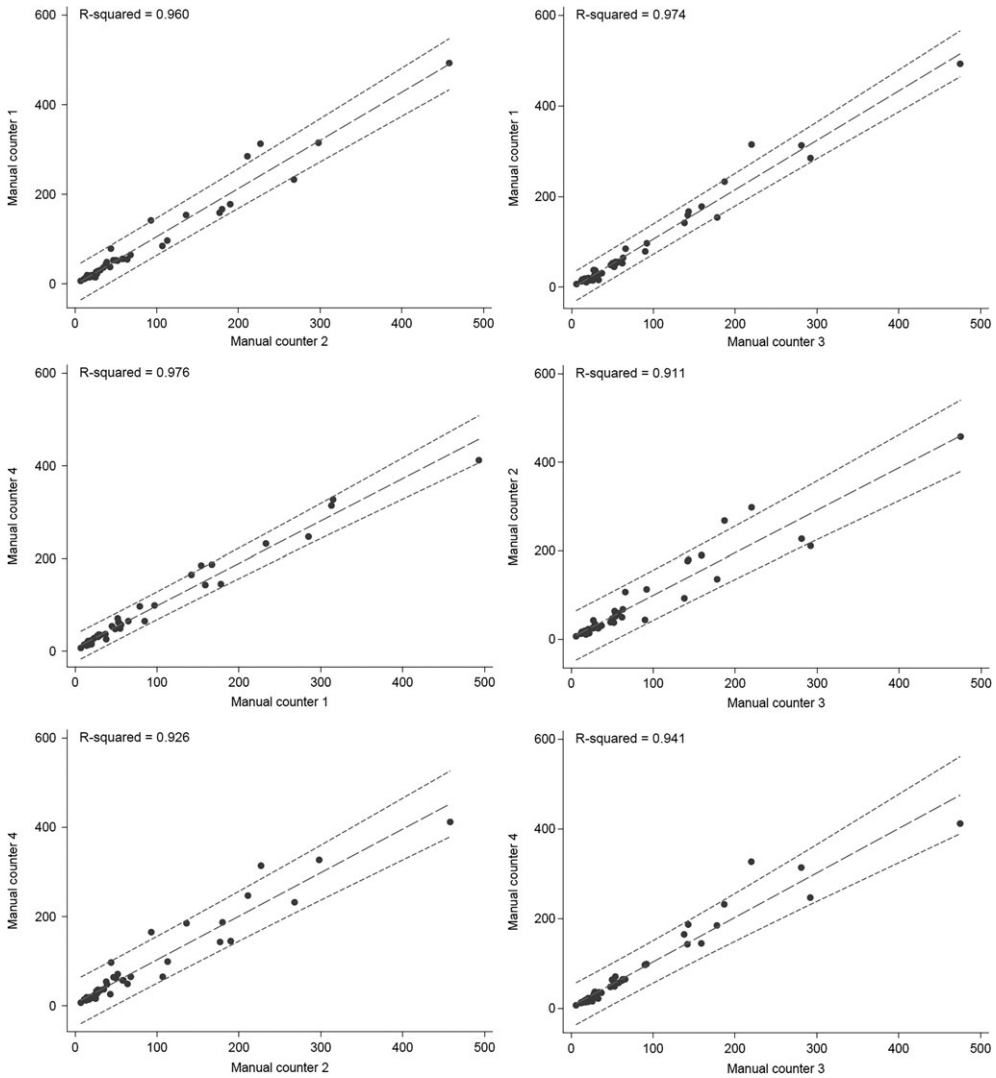

Figure 2. Linear regression analysis of pairwise comparisons for inter-counter validation analyses. The linear association between all manual counters (1–4) for the 45 validation images was assessed by linear regression models. The graphs demonstrate the fitted regression lines with 95% confidence forecast bands and the coefficient of determination (*R*-squared).

Information). Comparison of the whole data (Positive Cells-CellProfiler) set against the individual counters revealed that all counters were significantly in accord with CellProfiler (Table 2).

Comparisons Between CellProfiler Output Variables

CellProfiler is advantageous in that numerous variables may be simultaneously computed. In the current investigation, the following additional dataset variables were obtained and evaluated alongside the number of DAB-positive nuclei (Positive Cells-CellProfiler), number of DAB stained regions (DAB regions), area of DAB stained regions (DAB area), and the ratio between the DAB regions and total tissue area (DAB area masked) (Figure 3B, Table 2, and Supporting Information). Inter-comparisons between the different variables (DAB regions, DAB area, and DAB area masked), determined within CellProfiler, demonstrated significant agreement (Table 2). Interestingly, the relationship between the numbers of Positive Cells-CellProfiler to DAB regions, DAB area, and DAB area masked was strongly in agreement (r^2 = 0.938, 0.922, and 0.917, respectively), but importantly, outcomes between DAB regions and DAB area/area masked demonstrated reliable coefficients of determination (r^2 = 0.927, 0.904, and 0.888), which were similar to Positive Cells-CellProfiler (Table 2).

Discussion

CellProfiler has been extensively used in the study of fluorescently stained cells and tissues (7,8,11). However, few studies applied the software to the evaluation of chromogenic dye localization (13,14). In the current investigation, we primarily developed, validated, and evaluated a CellProfiler pipeline for the detection of CD4 DAB-IHC staining in oral

Table 1. Pairwise correlations between the manual counters for the validation set

		COUNTER 2	COUNTER 3	COUNTER 4
Counter 1	r^2	0.960	0.974	0.976
	95% confidence interval	0.982–1.168	1.000–1.180	0.818–1.010
Counter 2	r^2		0.911	0.926
	95% confidence interval		0.828–1.094	0.849–1.104
Counter 3	r^2			0.941
	95% confidence interval			0.818–1.164

Pairwise comparison analyses for counting of 45 images that constituted the validation set. Concordance was assessed by calculating the intra-image correlation, its 95% confidence interval, and the coefficient of determination. Full details of data output in the Supporting Information. r^2 = *R*-squared.

mucosal biopsies from cGvHD patients and compared against the gold standard manual counting. Indeed strong concordance between manual counting (validation and whole cohort counts) and digital image analysis resulted from the specific CD4-positive cell counting. However, within CellProfiler, additional data outputs were assessed including number of DAB regions, area of DAB staining, and area of DAB staining following masking of the input images, highlighting the program's versatility as this auxiliary information can be adapted to address specific questions.

With the rapid development of biological imaging techniques, computer-aided diagnostics has really emerged as a field together with whole side digital scanning, particularly for research approaches (24). There are many advantages to digital image analysis compared to current laborious manual counting. Manual counting is known to have a tendency toward numerous errors and requires estimation by multiple observers in a time-consuming approach (1). Within the current investigation, some discrepancies were apparent between counters based on their experience, which was noticeable in images with larger cell numbers. However, in sections with high-stained cell densities, representing extensive inflammatory infiltrate, CellProfiler was able to discern cell limits, declump, and identify individual cells. This is an important argument in favor of digital diagnostics. Current approaches for manual scoring systems between different disease states are often arbitrary, relying on percentage staining or improvised groupings that vary between studies (4,25,26). Thus, recent trends are moving toward novel approaches combining the percentage of antibody staining with visual features in a process driven by digital analyses (13). Examples include post-treatment diagnostics in gastric cancer and within current International Breast Cancer Guidelines (27,28).

When devising an image analysis protocol, numerous key features need consideration (reviewed by Ref. (5)). First, to address IHC as a quantitative assay, it is desirable to have a standardized protocol from the start to finish, including specimen fixation, embedding and sectioning to the specific antibody–antigen interactions, and detection of false positives (5,29–31). The current study employed CD4, a well-recognized transmembrane glycoprotein, expressed on normal thymocytes, T-helper cells, majority of mature peripheral T cells, and a subset of suppressor or cytotoxic T cells. However, problems arise concerning CD4 specificity as it has also been documented to also localize on dendritic cells (32,33). Thus, antigen–antibody interactions must be defined and well-characterized to produce reliable interpretation (1). Albeit not described herein, it should be noted that well-defined standard operating procedures have been employed for all IHC-associated protocols associated in this investigation. The second feature of critical importance for digital image analyses is post-analytical microscopy or digital scanning. Current recommendations for CellProfiler require that images are acquired as standardized as possible with constant lighting and minimal artefacts (34). However, this feature is not unique to CellProfiler and a consistent requirement across all imaging techniques. In this study, whole section imaging was performed followed by segmentation (image capture) of the sections to typically collect six or more images from each. The advantage of smaller images was that it provided a manageable image size for the manual counters that resembled approximately 30× magnification per FoV. Using the current CellProfiler pipeline, we have employed the use of the masking module to remove white regions or edges of tissues, which showed comparable results to DAB area. This approach of image masking would be of significant value when quantifying more dispersed staining, like extracellular matrix components and signaling molecules. Furthermore, we have subsequently developed the CellProfiler pipeline to evaluate whole section imaging through the combined use of automated image capture processes together with the automated masking procedure (data not included). This approach reduces any bias introduced when manually capturing images, improved accuracy by limiting the noise from empty white regions, and increased efficiency with a considerable reduction in processing time.

A big advantage to CellProfiler was the ability to devise pipelines for specific antibodies, which once established in a standardized protocol can be repeatedly used, a feature that may be of interest for routine diagnostics (14). Herein, parameters were optimized to enable not only counting of total number of DAB-positive cells but also DAB regions and DAB area/area-masked. The adaptability within the pipeline to add modules that allowed tissue compartmentalisation was important. For example, identification of individual nuclei stained with HTX, as well as the ability to separate cell

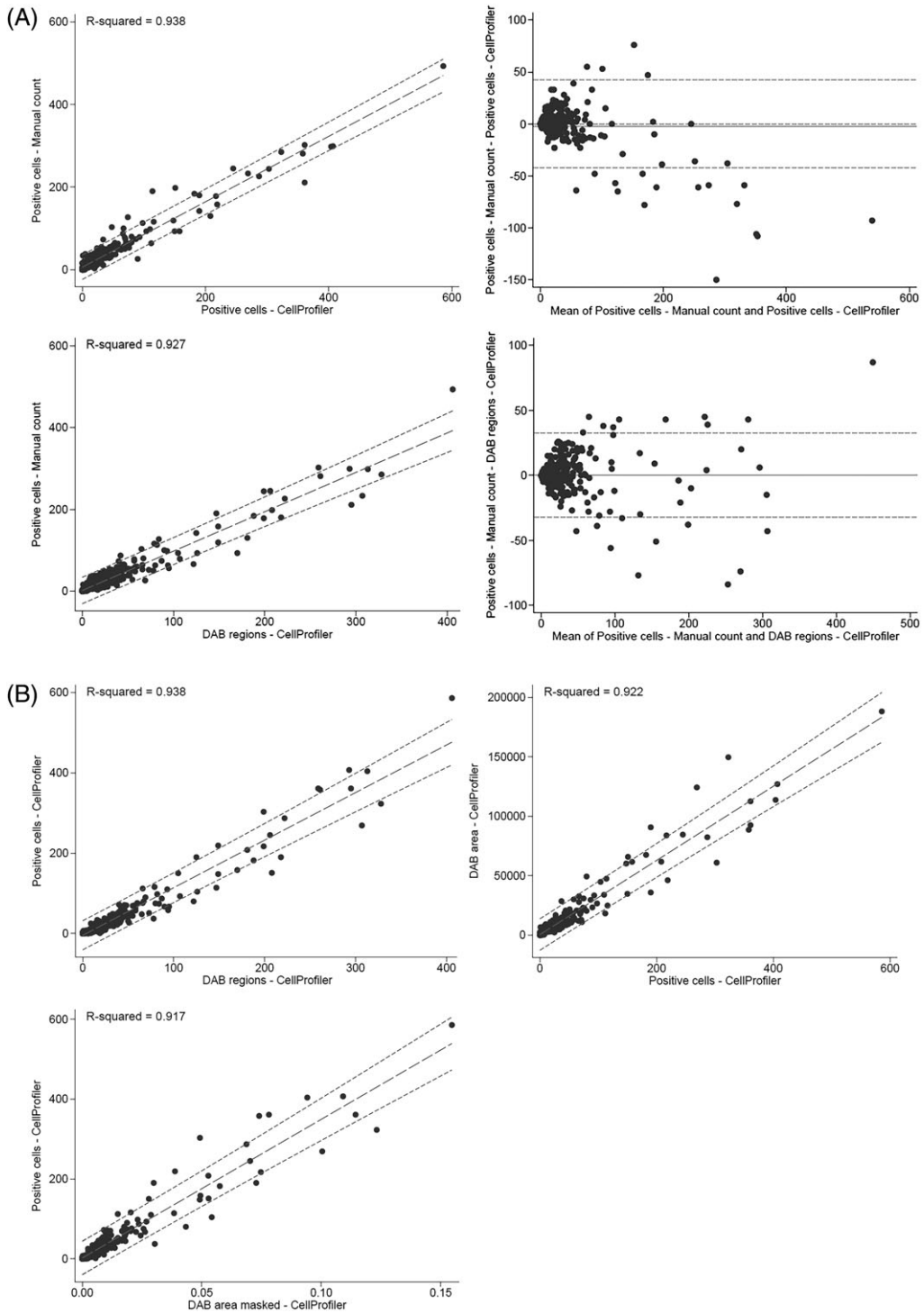

Figure 3. (A) Scatterplots with associated linear regression analyses of pairwise comparisons (left) and Bland–Altman plots (right) for Positive Cells-Manual Counting compared to Positive Cells-CellProfiler (upper) and DAB regions-CellProfiler (lower) (n = 299). The scatterplots demonstrate the fitted regression lines with 95% confidence forecast bands and the coefficient of determination (R-squared). The Bland–Altman plots show the degree of agreement between the manual counting and CellProfiler outputs. The vertical axis signifies the difference between the two methods and the horizontal axis the average of the two. The solid line represents the mean value and the dashed show $\pm$1.96 s. The similarity in width of the standard deviation for both Positive Cells-CellProfiler and DAB regions-CellProfiler suggests good agreement to the gold standard Positive Cells-Manual Counting. (B) Scatterplots and linear regression analysis of interobserver comparison between Positive Cells-CellProfiler and DAB regions-CellProfiler (left), DAB area (right) and DAB area-masked (below), images (n = 299) were assessed by linear regression models. The graphs demonstrate the fitted regression lines with 95% confidence forecast bands and the coefficient of determination (R-squared).

Table 2. Pairwise correlations between the manual counting against digital image analysis in CellProfiler

	CELLPROFILER IMAGE ANALYSIS			
	POSITIVE CELLS	DAB REGIONS	DAB AREA	DAB AREA MASKED
Manual counting				
Counter 1 (n = 130)	0.971	0.941	0.916	0.902
Counter 2 (n = 129)	0.921	0.935	0.929	0.911
Counter 3 (n = 130)	0.951	0.922	0.911	0.914
Counter 4 (n = 45)	0.969	0.957	0.925	0.913
Positive cells (n = 299)	0.938	0.927	0.904	0.888
Cell profiler image analysis				
Positive cells (n = 299)		0.938	0.922	0.917
DAB regions (n = 299)			0.977	0.972
DAB area (n = 299)				0.993

Pairwise comparison analyses on Positive Cells-Manual Counting (299 images randomly distributed across three counters [n = ~130] with the inclusion of counter 4 validation [n = 45]) against obtained Positive Cells-CellProfiler. In addition, pairwise comparison analyses of auxiliary data from CellProfiler, including the number of DAB stained regions (DAB regions), the area of DAB stained regions (DAB area), and the ratio between the DAB regions and total tissue area (DAB area masked). Concordance was assessed by calculating the intra-image correlation and its 95% confidence interval and the coefficient of determination (r^2 = R-squared). Full details of data output in the Supporting Information.

membranes from CD4 staining was vital to determine the number of positive cells. A major issue with digital IHC quantification is the definition of quantifiable parameters compared to pathologist's semiquantitate evaluation, so in addition to total cell counts suitable nonsubjective quantification tools are widely discussed, including detection limits of intensity and area stained (5). A strength of CellProfiler was the ability to tailor pipeline modules to address these issues. In this study, we were able to simultaneously determine DAB regions and DAB area/area-masked stained and relate these to pixel size of the area analyzed. There are significant benefits to using DAB areas over counts of positive cells; first, in cases where there may be excessive number of cells, such as inflammatory conditions, and the marker does not localize to these cell populations, the data output will be skewed and not truly reflect the DAB staining, and second when DAB staining is too intense difficulties arise in discerning nuclei and as a result cells may be excluded from analysis (5). Thus, it is a huge advantage that CellProfiler can provide definitive values or key parameters as staining area that may, in the future, be of value in assisting with clinical decision making.

Currently, digital tools will not replace the pathologist's human element in diagnostics in the near future as their experience is crucial to determining pattern recognition, a quintessential block in diagnostic pathology, but instead they complement the diagnostic procedure. Current trends toward machine learning and automated digital diagnostics are rapidly becoming the future (24,35,36). Such tools for research purposes proceed these developments and in the current study, we have demonstrated the significant potential of CellProfiler in the assessment of chromogenically stained tissues. CellProfiler allowed a rapid high processing capacity of large numbers of chromogenically stained chronic inflammatory tissue images that was reliable, accurate, and reproducible and highlights potential applications in research and routine pathological diagnostics.

Acknowledgment

The authors gratefully acknowledge Robert Heymann (Department of Dental Medicine, Karolinska Institutet, and Department of Oral and Maxillofacial Surgery Unit, Karolinska University Hospital) and Elisabeth Boström (Department of Dental Medicine, Karolinska Institutet, and Medical Dental Clinic Huddinge) for participating in the collection of the oral mucosa biopsies and SciLifeLab BioImage Informatics Facility.

Conflicts of Interest

The authors declare no conflicts of interest.

Literature Cited

1. Hamilton PW, Bankhead P, Wang YH, Hutchinson R, Kieran D, McArt DG, James J, Salto-Tellez M. Digital pathology and image analysis in tissue biomarker research. Methods. 2014;70:59–73.
2. Hanna MG, Pantanowitz L, Evans AJ. Overview of contemporary guidelines in digital pathology: what is available in 2015 and what still needs to be addressed? J Clin Pathol. 2015;68:499–505.
3. Bhargava R, Madabhushi A. Emerging themes in image informatics and molecular analysis for digital pathology. Annu Rev Biomed Eng. 2016;18:387–412.
4. Dobson L, Conway C, Hanley A, Johnson A, Costello S, O'Grady A, Connolly Y, Magee H, O'Shea D, Jeffers M, et al. Image analysis as an adjunct to manual HER-2 immunohistochemical review: a diagnostic tool to standardize interpretation. Histopathology. 2010;57:27–38.
5. Di Cataldo S, Ficarra E, Macii E. Computer-aided techniques for chromogenic immunohistochemistry: status and directions. Comput Biol Med. 2012;42:1012–1025.
6. Laurinavicius A, Plancoulaine B, Laurinaviciene A, Herlin P, Meskauskas R, Baltrusaityte I, Besusparis J, Dasevicius D, Elie N, Iqbal Y, et al. A methodology to ensure and improve accuracy of Ki67 labelling index estimation by automated digital image analysis in breast cancer tissue. Breast Cancer Res. 2014;16:R35.
7. Carpenter AE, Jones TR, Lamprecht MR, Clarke C, Kang IH, Friman O, Guertin DA, Chang JH, Lindquist RA, Moffat J, et al. CellProfiler: image analysis software for identifying and quantifying cell phenotypes. Genome Biol. 2006;7:R100.
8. Lamprecht MR, Sabatini DM, Carpenter AE. CellProfiler: free, versatile software for automated biological image analysis. Biotechniques. 2007;42:71–75.
9. Ball SG, Shuttleworth A, Kielty CM. Inhibition of platelet-derived growth factor receptor signaling regulates Oct4 and Nanog expression, cell shape, and mesenchymal stem cell potency. Stem Cells. 2012;30:548–560.
10. Bettenworth D, Lenz P, Krausewitz P, Bruckner M, Ketelhut S, Domagk D, Kemper B. Quantitative stain-free and continuous multimodal monitoring of wound healing in vitro with digital holographic microscopy. PLoS One. 2014;9:e107317.
11. Diem K, Magaret A, Klock A, Jin L, Zhu J, Corey L. Image analysis for accurately counting CD4+and CD8+ T cells in human tissue. J Virol Methods. 2015;222:117–121.
12. Paulik R, Micsik T, Kiszler G, Kaszal P, Szekely J, Paulik N, Varhalmi E, Premusz V, Krenacs T, Molnar B. An optimized image analysis algorithm for detecting nuclear signals in digital whole slides for histopathology. Cytometry Part A. 2017;91A:595–608.
13. Campbell MJ, Baehner F, O'Meara T, Ojukwu E, Han B, Mukhtar R, Tandon V, Endicott M, Zhu Z, Wong J, et al. Characterizing the immune microenvironment in high-risk ductal carcinoma in situ of the breast. Breast Cancer Res Treat. 2017;161:17–28.

14. Iacobaeus E, Sugars RV, Andren AT, Alm JJ, Qian H, Frantzen J, Newcombe J, Alkass K, Druid H, Bottai M, et al. Dynamic changes in brain mesenchymal perivascular cells associate with multiple sclerosis disease duration, active inflammation, and demyelination. Stem Cells Transl Med. 2017;6:1840–1851.
15. Schubert MM, Williams BE, Lloid ME, Donaldson G, Chapko MK. Clinical assessment scale for the rating of oral mucosal changes associated with bone-marrow transplantation. Development of an oral mucositis index. Cancer. 1992;69:2469–2477.
16. Filipovich AH, Weisdorf D, Pavletic S, Socie G, Wingard JR, Lee SJ, Martin P, Chien J, Przepiorka D, Couriel D, et al. National Institutes of Health Consensus Development Project on criteria for clinical trials in chronic graft-versus-host disease: I. Diagnosis and staging working group report. Biol Blood Marrow Transpl. 2005;11:945–956.
17. Otsu N. Threshold selection method from gray-level histograms. IEEE Trans Syst Man Cybern. 1979;9:62–66.
18. Kish L. Generalizations for nonrandom probability sampling. J Am Stat Assoc. 1965;60:665–665.
19. Donner A. A review of inference procedures for the intraclass correlation-coefficient in the one-way random effects model. Int Stat Rev. 1986;54:67–82.
20. Mandrekar JN. Measures of interrater agreement. J Thorac Oncol. 2011;6:6–7.
21. Huber PJ. *The Behavior of Maximum Likelihood Estimates Under Nonstandard Conditions*. Berkeley: University of California Press, 1967;p. 221–233.
22. Giavarina D. Understanding Bland Altman analysis. Biochem Med. 2015;25:141–151.
23. Koopman T, Buikema HJ, Hollema H, de Bock GH, van der Vegt B. Digital image analysis of Ki67 proliferation index in breast cancer using virtual dual staining on whole tissue sections: clinical validation and inter-platform agreement. Breast Cancer Res Treat. 2018;169:33–42.
24. Janowczyk A, Madabhushi A. Deep learning for digital pathology image analysis: a comprehensive tutorial with selected use cases. J Pathol Inform. 2016;7:29.
25. Bazarsad S, Zhang X, Kim KY, Illeperuma R, Jayasinghe RD, Tilakaratne WM, Kim J. Identification of a combined biomarker for malignant transformation in oral submucous fibrosis. J Oral Pathol Med. 2017;46:431–438.
26. Nguyen AN, Moore J, O'Dwyer J, Philpot S. Automated cancer registry notifications: validation of a medical text analytics system for identifying patients with cancer from a state-wide pathology repository. AMIA Annu Symp Proc. 2016;2016:964–973.
27. Bilous M, Ades C, Armes J, Bishop J, Brown R, Cooke B, Cummings M, Farshid G, Field A, Morey A, et al. Predicting the HER2 status of breast cancer from basic histopathology data: an analysis of 1500 breast cancers as part of the HER2000 International Study. Breast. 2003;12:92–98.
28. Hofmann M, Stoss O, Shi D, Buttner R, van de Vijver M, Kim W, Ochiai A, Ruschoff J, Henkel T. Assessment of a HER2 scoring system for gastric cancer: results from a validation study. Histopathology. 2008;52:797–805.
29. Seidal T, Balaton AJ, Battifora H. Interpretation and quantification of immunostains. Am J Surg Pathol. 2001;25:1204–1207.
30. Taylor CR. Standardization in immunohistochemistry: the role of antigen retrieval in molecular morphology. Biotech Histochem. 2006;81:3–12.
31. Taylor CR, Levenson RM. Quantification of immunohistochemistry—issues concerning methods, utility and semiquantitative assessment II. Histopathology. 2006;49:411–424.
32. Hasseus B, Jontell M, Brune M, Johansson P, Dahlgren UI. Langerhans cells and T cells in oral graft versus host disease and oral lichen planus. Scand J Immunol. 2001;54:516–524.
33. Walsh LJ, Parry A, Scholes A, Seymour GJ. Modulation of Cd4 antigen expression on human gingival langerhans cells by gamma interferon. Clin Experim Immunol. 1987;70:379–385.
34. Bray MA, Vokes MS, Carpenter AE. Using CellProfiler for automatic identification and measurement of biological objects in images. Curr Protoc Mol Biol. 2015;109:14 17:1–13.
35. Bray MA, Carpenter AE. Quality control for high-throughput imaging experiments using machine learning in CellProfiler. Methods Mol Biol. 1683;2018:89–112.
36. Djuric U, Zadeh G, Aldape K, Diamandis P. Precision histology: how deep learning is poised to revitalize histomorphology for personalized cancer care. NPJ Precis Oncol. 2017;1:22.